Contribution from the Department of the Geophysical Sciences, The University of Chicago, Chicago, Illinois 60637

Parwelite, $Mn^{II}_{10}Sb^{V}_{2}As^{V}_{2}Si_2O_{24}$, a Complex Anion-Deficient Fluorite Derivative Structure

PAUL BRIAN MOORE* and TAKAHARU ARAKI

Received December 1, 1976 AIC60863A

Parwelite, asymmetric unit $Mn^{II}_{8.30}Ca_{0.36}Mg_{1.50}Sb^{V}_{1.84}As^{V}_{2.00}Si_{2.00}O_{24.00}$, was studied in detail by three-dimensional x-ray diffractometry. It possesses space group *Aa*, with $a = 10.048$ (2) Å, $b = 19.418$ (5) Å, $c = 9.735$ (2) Å, and $\beta = 95.83$ (1)°; $R = 0.048$ ($R_w = 0.049$) for 1665 independent reflections. Reflections were collected on a Picker automated four-circle diffractometer and the structure was solved by Fourier, chemical intuitive, and least-squares refinement techniques. The compound is an anion-deficient fluorite derivative structure ($a = 2a_F$, $b = 4a_F$, $c = 2a_F$) of extraordinary complexity and the end-member asymmetric unit can be written $Mn^{II}_{10}Sb^{V}_{2}As^{V}_{2}Si_2O_{24}\square_8$, where □'s are anion vacancies. The use of sheet groups and pole groups assists in relating its structure to other fluorite derivatives. Average polyhedral distances (the coordination number written in bracketed superscripts) are $^{[6]}$Sb(1)–O = 1.99, $^{[6]}$Sb(2)–O = 1.99, $^{[6]}$M(1)–O = 2.21, $^{[6]}$M(2)–O = 2.21, $^{[6]}$M(3)–O = 2.23, $^{[6]}$M(4)–O = 2.24, $^{[6]}$M(5)–O = 2.21, $^{[6]}$M(6)–O = 2.17, $^{[4]}$M(7)–O = 2.07, $^{[8]}$M(8)–O = 2.42, $^{[5]}$M(9)–O = 2.09, $^{[5]}$M(10)–O = 2.12, $^{[4]}$Si(1)–O = 1.63, $^{[4]}$Si(2)–O = 1.64, $^{[4]}$As(1)–O = 1.68, and $^{[4]}$As(2)–O = 1.68 Å.

Introduction

Parwelite, $(Mn,Mg,Ca)^{V}_{5}Sb^{V}As^{V}SiO_{12}$, is a highly complex oxide which was recently described[1] as a new species from the famous manganese–iron oxide deposits of Långban, Sweden. Over 20 elements play a geochemically significant role in this deposit, resulting in crystal–chemical relationships of such extraordinary complexity that no less than 250 discrete mineral species have been described.[2]

Parwelite occurs as hard, brittle subadamantine rounded crystals of complex morphology up to 1 cm in dimension, ranging from pale brown to orange and much resembling garnets for which it was at first mistaken. It occurs in a high-temperature skarn assemblage associated with oxides, silicates, arsenites, and arsenates of Mn^{2+}, Mn^{3+}, Sb^{3+}, Sb^{5+}, Fe^{3+}, Ca^{2+}, Mg^{2+}, Be^{2+}, and Al^{3+} all embedded in a recrystallized dolomite matrix. Unlike the synthetic inorganic chemist who proceeds from controlled systems with but few components, the mineralogist is usually faced with polycomponent systems of great complexity from which thermochemical and crystal–chemical relationships must be inferred.

We were drawn to the parwelite problem owing to its apparent relationship with braunite and bixbyite, phases which were earlier discussed in considerable detail.[3-5] Of more interest is the relationship of this phase to the fluorite structure type and its myriad anion-deficient derivatives such as braunite, bixbyite, pyrochlore, calzirtite, armangite, magnussonite, murataite, scheelite, Pr_6O_{11}, phases in the system CeO_2–Ce_2O_3, and many others.

Experimental Procedure

The earlier study[1] reported the cell parameters in Table I. Redetermination of these parameters by precession photography and subsequently by single-crystal diffractometry revealed an incorrect space group determination which resulted from missetting of the Weissenberg photographs in the earlier investigation. This was further confirmed by examination of the original photographs.

Two partial chemical analyses were reported for parwelite[1] and were obtained from emission spectrographic and electron probe analytical techniques. Formal charge states had to be inferred in the absence of other direct evidence and the cell contents were reported as $Mn_{32.90}Ca_{1.41}Pb_{0.09}Fe_{0.04}Mg_{5.88}Sb^{III}_{7.24}As^{III}_{11.74}Si_{6.15}O_{81.09}$. Uncertainties were raised about the accuracy of the As and Si determinations. The success of the present structure determination allows for unambiguous reinterpretation of the formula. We show herein that Sb^{5+} and As^{5+} are the formal charge states for these cations and that the cell contains a total of 64 cations and 96 oxide anions. Furthermore, successful refinement of the structure parameters leaves little doubt that 8 As^{5+} and 8 Si^{4+} occur in the cell and that any substitutions at these sites must be small. Recasting the unit formula ($Z = 4$) to account for the present observations leads to $Mn^{II}_{8.30}Ca_{0.36}Mg_{1.50}Sb^{V}_{1.84}As^{V}_{2.00}Si_{2.00}O_{24.00}$. It is seen in Table I that the computed density based on this formula is in excellent agreement with the observed value. The end-member composition to which parwelite can be referred is $Mn^{II}_{10}Sb^{V}_{2}As^{V}_{2}Si_2O_{24}$. Owing to substituents in place of Mn, these sites are labeled "M" in this study.

Table I. Parwelite Experimental Details

(A) Crystal Cell Data

Ref	This study	Ref 1[a]
a, Å	10.048 (2)	9.76 (2)
b, Å	19.418 (5)	19.32 (2)
c, Å	9.735 (2)	10.06 (2)
β, deg	95.83 (1)	95.90 (10)
V, Å^3	1889.5	
Space group	*Aa*	
Z	4	
Formula	$Mn^{II}_{8.30}Ca_{0.36}Mg_{1.50}Sb^{V}_{1.84}As^{V}_{2.00}Si_{2.00}O_{24.00}$	
ρ(calcd), g cm^{-3}	4.64	
ρ(obsd), g cm^{-3}	4.62	
μ, cm^{-1}	67.4	

(B) Intensity Measurements

Crystal size, mm: ellipsoid, 0.117 × 0.182 × 0.208
Crystal orientation: ϕ axis = [010]
Background counts: stationary, 10 s at beginning and end of scan
Radiation: Mo Kα, Kevex Si–Li solid-state detector
Independent F_o: 1665

(C) Refinement of the Structure

R	0.048
R_w	0.049
Goodness of fit	1.000

[a] The observed density, ρ(obsd), is also quoted from this source.

We are grateful to Dr. G. D. Brunton of Oak Ridge National Laboratory for the data collection. A single crystal was ground into an ellipsoid 0.117 × 0.182 × 0.208 mm in dimensions. Unit cell parameters were obtained from 36 independent high-angle reflections and refined to the results in Table I. The data were collected on a Picker four-circle goniostat using a Kevex Si–Li solid-state detector. The radiation was unfiltered Mo Kα with Mo Kβ eliminated by a 400 eV wide pulse-height analyzer window. The (404) reflection was selected as the reference and was sampled every 20th scan. The net count range of this standard was from 151 000 to 160 000. The reflections were step-scanned in increments of 0.03 in 2θ over a total of $2\theta = (2.1 \times 114.6\Delta\lambda/\lambda)°$. Each step was counted for 2 s and the background on each side of the reflection for 10 s.

The variance whose reciprocal was used in the least-squares adjustment of the structure parameters was $\sigma^2(F_o^2) = [T + B + (0.03(T - B))^2]/A(Lp)^2$, where T is total counts, B is background counts, A

Table II. Parwelite Powder Data[a]

I(obsd)	*I*(calcd)	*d*(obsd)	*d*(calcd)	*hkl*
30	23	9.646	9.709	$0\bar{2}0$
10	8	6.815	6.864	$\bar{1}11$
12	11	4.973	4.998	200
44	17	4.831	4.854	040
	6		4.842	002
15	7	4.314	4.333	$0\bar{2}2$
	8		3.433	$\bar{1}51$
55	12	3.419	3.432	$\bar{2}22$
	10		3.428	$0\bar{4}2$
5	6	3.196	3.209	$\bar{3}11$
15	12	3.117	3.126	$\bar{1}13$
100	100	2.916	2.927	$\bar{2}42^b$
100	94	2.729	2.737	242^b
15	13	2.491	2.499	400
40	17	2.421	2.427	080
	11		2.421	004
25	12	2.310	2.315	$26\bar{2}$
10	10	1.832	1.835	$\bar{4}04^b$
10	7	1.800	1.803	$42\bar{4}$
25	18	1.738	1.741	480^b
25	19	1.712	1.714	084^b
15	13	1.656	1.657	$\bar{4}04^b$
5	7	1.541	1.543	$\bar{6}42^b$
5	5	1.504	1.506	$\bar{2}46^b$
15	6	1.479	1.481	$\bar{2},12,2^b$
10	6	1.456	1.458	642^b
10	6	1.453	1.454	$2,12,2^b$
10	9	1.426	1.426	246^b
5	5	1.368	1.368	484

[a] *I*(calcd) > 4 were included. [b] These indices refer to fluorite-type reflections (see text). The powder sample was not corrected for absorption.

is absorption correction, and *Lp* is the Lorentz and polarization correction.

A diffractometer trace of the parwelite powder pattern was obtained using Cu Kα radiation with a graphite monochromator and a scan speed of $^1/_2$° min^{-1}. From the refined crystal structure, a calculated powder pattern was obtained and these results are presented in Table II.

Structure Determination and Refinement

Programs used in determining the structure were earlier listed.[6] Solution of the parwelite crystal structure was acknowledged as a special challenge owing to the pronounced fluorite substructure. Indeed, inspection of Table II shows that the fluorite substructure dominates the intensities, the fluorite lines splitting as follows: $\{111\}_F$ = {(242), $(\bar{2}42)$}$_p$; $\{220\}_F$ = {(480), (404), $(\bar{4}04)$, (084)}$_p$; $\{311\}_F$ = {(642), $(\bar{6}42)$, (2,12,2), $(\bar{2},12,2)$, (246), $(\bar{2}46)$}$_p$; $\{400\}_F$ = {(800), (008), (0,16,0)}$_p$; $\{331\}_F$ = {(6,12,2), $(\bar{6},12,2)$, (646), $(\bar{6}46)$}$_p$; $\{422\}_F$ = {(884), $(\bar{8}84)$, (488), $(\bar{4}88)$, (4,16,4), $(\bar{4},16,4)$}$_p$. Clearly, we were forced to solve the substructure and then, on the grounds of chemical reasoning, order the cations of large atomic member in such a way to correctly phase the reflections contributing to the superstructure. Assuming that Sb^{5+} was ordered over octahedral sites, it was possible to interpret the Patterson function, $P(uvw)$, on the basis of the dominant Sb–Sb′, Sb–As, and Sb–Mn vectors. The ordering schemes for Sb and As were obtained in this manner. The Mn atoms were distributed over the remaining cation positions in a fluorite-type arrangement. At this stage, the structure was believed to be centrosymmetric, supported by the $P(y)$ test on general reflections,[7] and the initial coordinate parameters were utilized as input for a trial β synthesis.[8]

The first β map revealed most of the oxygen atoms and a pronounced sheetlike octahedral structure at $y = 0$. Addition of the oxygen atoms sharpened the subsequent map but it was not yet possible to ascertain the distributions of Si atoms which we asserted would appear in tetrahedral coordination by the oxygen atoms. Unfortunately, parwelite possesses not one kind of superstructure but two and the present model admitted correct phasing only for the $h, k, l = 2n$ reflections. The crucial step was then to "force" the Si positions; indeed, weak "Mn" densities at $y = {}^1/_8$ suggested the presence of Si instead and these were placed in tetrahedral coordination in such a manner that the $h, k, l \neq 2n$ reflections would be nonzero. The trial model placed Si(1) at $\sim{}^1/_4$, $^1/_8$, 0 and Si(2) at $\sim{}^3/_4$, $^1/_8$, $^1/_2$. Successive β iterations revealed the remaining oxygen atoms but trial least-squares refinements did not converge below $R = 0.33$ for all reflections.

The problem was traced to the oxygen environment about the As atoms. Fourier synthesis showed the presence of possible disorder, with the two tetrahedra each split into pairs. This indicated that the structure was in fact not centrosymmetric but acentric. A choice was then made, with one of the two split tetrahedra selected as input. Refinement in space group *Aa* led to rapid convergence; owing to high correlations, we were forced to perform two blocked-matrix refinements, alternating between atoms related by pseudocentrosymmetry. Final refinement involved variation of one scale factor, one secondary extinction coefficient, 10 site population parameters (M(1) through M(10)), 118 atomic coordinate parameters, and 40 isotropic thermal vibration parameters, yielding a data to variable parameters ratio of 6:1. Refinement converged to $R = 0.048$ and $R_w = 0.049$ where

$$R = \frac{\Sigma||F_o| - |F_c||}{\Sigma|F_o|}$$

$$R_w = \left[\frac{\Sigma w(|F_o| - |F_c|)^2}{\Sigma w F_o{}^2}\right]^{1/2}$$

The final cycle minimized $\Sigma w||F_o| - |F_c||^2$ where $w = \sigma F^{-2}$. We employed scattering curves[9] for Mn^{2+}, Mg^{2+}, Sb^{5+}, As^{5+}, Si^{4+}, and O^- and anomalous dispersion corrections,[10] f'', for Mn^{2+}, Sb^{5+}, and As^{5+}. The secondary extinction correction[11] refined to $c_0 = 1.7\ (8) \times 10^{-8}$. Atomic coordinate and isotropic thermal vibration parameters for all 40 atoms in the asymmetric unit appear in Table III.

Table IV lists the results of the site population refinements over the M(1) through M(10) positions and the ideal and real oxygen coordination numbers for the cations, to be discussed subsequently. Site populations were assessed by applying scattering curves for Mn^{2+} and Mg^{2+} at the M positions.[12] The refinement suggests a total of 1.82 Mg/formula unit which compares favorably with Mg + Ca = 1.86 according to the chemical analysis. We suspect that Ca^{2+} quantitatively substitutes at the M(8) site with eight-coordination. It is important to note that M(9) and M(10), which are five-coordinate sites, preferentially accept Mg^{2+}.

Although convergence is excellent for such a complex structure as parwelite, the isotropic temperature factors, particularly for oxygen, show a considerable range (from 0.3 to 3.3 Å^2). This doubtless arises from the relatively low data-to-variable parameter ratio and the high correlations inherent in the crystal structure. For this reason, we assert that the thermal parameters probably have little physical meaning and, as such, can only be "improved" through collection of a much larger data set, say from Ag Kα radiation instead of Mo Kα. Final difference Fourier synthesis did not reveal any unusual features beyond very minor residuals of at most two electrons.

The polyhedral bond distances and angles are listed in Table V.

Description of the Structure

Relation to the Fluorite Parent Structure: Group Theory. The atomic arrangement of parwelite is extremely complex and a description of the coordination polyhedra alone will not suffice since it is a derivative structure of the well-known fluorite $^{[8]}Ca^{[4]}F_2$, $a = 5.46$ Å, $Z = 4$, $Fm3m$, arrangement. Fluorite is the parent structure of a large number of highly refractory fluorides, oxyfluorides, and oxides; these structures obtain by ordered removal of anions, creating vacancies (□), with a variety of cations ordered over the available cation positions in fluorite. Thus, we are concerned with the series $X_r\phi_{2r}$–$X_r\phi_{2r-s}\square_s$, where X are the cations of which there are r in the cell, ϕ are the anions, and □ the ordered vacancies over these anion positions of which there are s in the cell. For fluorite, $r = 4$. Any multiple cell derivative of the fluorite structure possesses a multiple cell: $a = ma_F$, $b = na_F$, $c = pa_F$; and the total number of cations is $4mnp$. For parwelite, $(m, n, p) = (2, 4, 2)$ so there are 64 cations in the cell (40 Mn^{2+} + 8 Sb^{5+} + 8 As^{5+} + 8 Si^{4+}), 96 O^{2-} anions, and 32 vacancies. Thus, the asymmetric unit ($Z = 4$) can be written $Mn^{II}_{10}Sb^{V}_{2}As^{V}_{2}Si^{IV}_{2}O_{24}\square_8$. The problem then reduces to inquiring how these vacancies are ordered and inquiring about

Table III. Atomic Coordinate and Isotropic Thermal Vibration Parameters for Parwelite[a]

	x	y	z	B, Å²	x	y	z	D, Å
Sb(1)	0.0000	0.9954 (1)	0.0000	0.87 (4)	0	0	0	0.09
Sb(2)	0.0016 (1)	0.9956 (1)	0.5009	0.90 (3)	0	0	1/2	0.09
M(1)	0.2529 (6)	0.0026 (3)	0.2498 (6)	1.20 (6)	1/4	0	1/4	0.06
M(2)	0.7551 (6)	0.9973 (3)	0.7536 (5)	1.13 (6)	3/4	0	3/4	0.08
Si(1)	0.2480 (8)	0.1218 (5)	0.0055 (8)	2.02 (14)	1/4	1/8	0	0.09
Si(2)	0.7609 (6)	0.1194 (3)	0.4978 (6)	0.33 (9)	3/4	1/8	1/2	0.16
M(3)	0.0076 (5)	0.1102 (2)	0.2476 (5)	1.24 (6)	0	1/8	1/4	0.30
M(4)	0.5008 (5)	0.1423 (1)	0.2517 (5)	1.18 (5)	1/2	1/8	1/4	0.34
M(5)	0.2456 (4)	0.1034 (2)	0.4991 (5)	1.20 (12)	1/4	1/8	1/2	0.42
M(6)	0.7588 (4)	0.1035 (2)	0.0044 (4)	0.87 (11)	3/4	1/8	0	0.43
M(7)	0.0004 (5)	0.1311 (1)	0.7502 (6)	1.19 (5)	0	1/8	3/4	0.12
M(8)	0.5070 (5)	0.1259 (1)	0.7479 (5)	1.21 (6)	1/2	1/8	3/4	0.08
As(1)	0.9333 (3)	0.2546 (1)	0.0462 (3)	1.29 (5)	0	1/4	0	0.85
As(2)	0.0663 (3)	0.2550 (1)	0.4590 (3)	1.24 (5)	0	1/4	1/2	0.82
M(9)	0.2646 (5)	0.2547 (3)	0.2224 (6)	0.65 (14)	1/4	1/4	1/4	0.33
M(10)	0.7403 (6)	0.2545 (3)	0.2874 (6)	1.55 (14)	3/4	1/4	1/4	0.40
O(1)	0.1460 (12)	0.0674 (7)	0.0843 (13)	0.4 (2)	1/8	1/16	1/8	0.48
O(2)	0.5998 (21)	0.0672 (12)	0.1307 (22)	2.6 (4)	5/8	1/16	1/8	0.28
O(3)	0.8924 (13)	0.0378 (7)	0.1313 (13)	0.3 (2)	7/8	1/16	1/8	0.51
O(4)	0.1159 (18)	0.0316 (10)	0.3661 (18)	1.8 (3)	1/8	1/16	3/8	0.61
O(5)	0.4075 (13)	0.0696 (8)	0.3728 (14)	0.3 (2)	3/8	1/16	3/8	0.36
O(6)	0.8689 (15)	0.0669 (8)	0.4379 (16)	1.6 (3)	7/8	1/16	3/8	0.63
O(7)	0.1022 (20)	0.0575 (11)	0.6330 (20)	2.6 (4)	1/8	1/16	5/8	0.27
O(8)	0.3920 (13)	0.0428 (7)	0.6393 (13)	0.2 (2)	3/8	1/16	5/8	0.44
O(9)	0.6524 (13)	0.0716 (8)	0.5793 (14)	0.7 (3)	5/8	1/16	5/8	0.57
O(10)	0.3580 (15)	0.0732 (9)	0.9407 (16)	1.3 (3)	3/8	1/16	7/8	0.71
O(11)	0.6143 (22)	0.0436 (13)	0.8734 (22)	3.3 (4)	5/8	1/16	7/8	0.38
O(12)	0.9090 (12)	0.0637 (7)	0.8714 (13)	0.2 (2)	7/8	1/16	7/8	0.35
□(1)					3/8	1/16	1/8	
□(2)					5/8	1/16	3/8	
□(3)					7/8	1/16	5/8	
□(4)					1/8	1/16	7/8	
O(13)	0.3142 (18)	0.1647 (10)	0.1330 (18)	1.5 (3)	3/8	3/16	1/8	0.76
O(14)	0.5755 (21)	0.2421 (11)	0.1303 (23)	2.6 (4)	5/8	3/16	1/8	1.17
O(15)	0.9020 (15)	0.1757 (9)	0.1093 (15)	1.1 (3)	7/8	3/16	1/8	0.40
O(16)	0.1128 (17)	0.1799 (11)	0.3890 (17)	1.9 (3)	1/8	3/16	3/8	0.24
O(17)	0.4249 (16)	0.2411 (8)	0.3726 (17)	0.9 (3)	3/8	3/16	3/8	1.16
O(18)	0.6915 (17)	0.1614 (10)	0.3677 (17)	1.2 (3)	5/8	3/16	3/8	0.85
O(19)	0.3276 (17)	0.1935 (9)	0.6062 (17)	2.0 (3)	3/8	3/16	5/8	0.51
O(20)	0.5808 (15)	0.2145 (8)	0.6259 (15)	1.1 (3)	5/8	3/16	5/8	0.69
O(21)	0.8361 (17)	0.1644 (10)	0.6220 (18)	2.0 (3)	7/8	3/16	5/8	0.59
O(22)	0.1595 (13)	0.1612 (8)	0.8838 (13)	0.3 (2)	1/8	3/16	7/8	0.62
O(23)	0.4229 (17)	0.2224 (9)	0.8859 (18)	2.1 (3)	3/8	3/16	7/8	0.83
O(24)	0.6786 (14)	0.1866 (8)	0.8924 (15)	0.8 (2)	5/8	3/16	7/8	0.55
□(5)					1/8	3/16	1/8	
□(6)					7/8	3/16	3/8	
□(7)					1/8	3/16	5/8	
□(8)					7/8	3/16	7/8	

[a] The ideal fluorite coordinates are listed as fractions and the atom displacements away from these positions are listed under "D". Estimated standard errors in parentheses refer to the last digit. The eight nonequivalent anion holes, □, are also listed.

the coordination number for the cations as a consequence of this ordering.

The vehicles for classifying the anion-deficient fluorite derivative structures were explained in detail[5] based on a study of the related structure of braunite, $^{[8]}Mn^{II}(^{[6]}Mn^{III}_6)$-$^{[4]}Si^{IV}O_{12}\square_4$. The fluorite structure can be conceived as a checkerboard of edge-sharing cubes in the plane upon which similar checkerboards are stacked by further edge-sharing. The problem then reduces to the graphical enumeration of vacancies over an asymmetric unit of checkerboards. Utilizing the enumeration theorem of Pólya,[17] we classified[5] the possible ordered vacancies over the vertices of the cubic domain and the highest point symmetries of the resultant inventory of patterns. These discrete arrangements were then used as "players" on a checkerboard, the rules of which were discussed in the earlier study as a cooperative lattice game. Each conclusion of a cooperative lattice game is a potential structure type. In this study we adopt the nomenclature of the earlier investigation.

The first step is to establish the *ideal* checkerboards for parwelite. The space group *Aa* and $n = 4$ require the definition of three nonequivalent checkerboards at $y \approx 0$, $^1/_8$, and $^1/_4$. These are assessed directly from the atomic coordinates in Table III and are featured in the Figure 1 series. Since no displacements of the oxygens in the real structure are greater than 1.2 Å away from the ideal fluorite arrangement, it is possible to unambiguously assign their ideal positions. It is seen that Sb(1), Sb(2), M(1), M(2), M(9), and M(10) have arrangement $u^6d^2(3)$; M(3), M(4), As(1), and As(2) have $u^6d^2(2)$; M(5) and M(6) have $u^7d^1(1)$; M(7) has $u^4d^4(4)$; M(8) has u^8; and Si(1) and Si(2) have $u^5d^3(3)$. These, and the consequent maximal coordination numbers, are summarized in Table IV.

Examining the checkerboards further, we see that Figure 1a at $z = 0$ can be referred to sheet group *pmam*, $a' = (a + c)/4$, $c' = (a - c)/2$; Figure 1b at $z = ^1/_4$ is *pcam*, $a' = a$, $c' = c/2$; and Figure 1c at $z = ^1/_8$ is *p*2, $a' = a$, $c' = c$. Now, taking the intersections of these sheet groups, S{*pmam*} ∩

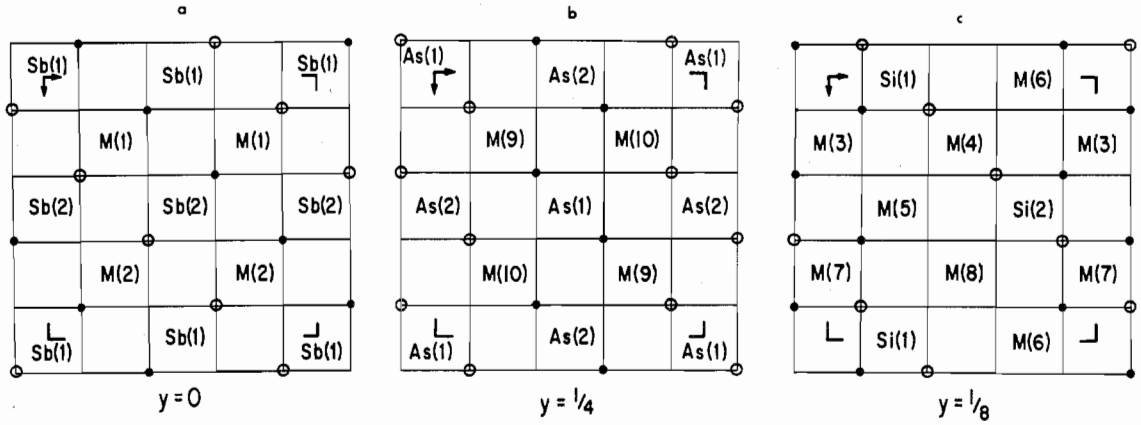

Figure 1. Three nonequivalent checkerboards in the parwelite crystal structure. Vacancies on the cube vertices above the plane are represented as solid disks; those below the plane, as open circles. The centers of the cubes are labeled according to the cations populating them: (a) the checkerboard at $y = 0$; (b) the checkerboard at $y = {}^1/_4$; (c) the checkerboard at $y = {}^1/_8$.

Table IV. Site Populations and Ideal and Real Coordination Numbers for Parwelite[a]

Atom	Mn^{2+}	Mg^{2+}	Ideal no.	Real no.	Code
M(1)	0.82 (2)	0.18	6	6	$u^6d^2(3)$
M(2)	0.91 (2)	0.09	6	6	$u^6d^2(3)$
M(3)	0.88 (1)	0.12	6	6	$u^6d^2(2)$
M(4)	0.94 (1)	0.06	6	6	$u^6d^2(2)$
M(5)	0.82 (3)	0.18	7	6	u^7d^1
M(6)	0.87 (3)	0.13	7	6	u^7d^1
M(7)	0.92 (1)	0.08	4	4	$u^4d^4(4)$
M(8)	0.83 (2)	0.17	8	8	u^8
M(9)	0.51 (3)	0.49	6	5	$u^6d^2(3)$
M(10)	0.68 (3)	0.32	6	5	$u^6d^2(3)$
1.00 Sb(1)			6	6	$u^6d^2(3)$
1.00 Sb(2)			6	6	$u^6d^2(3)$
1.00 As(1)			6	4	$u^6d^2(2)$
1.00 As(2)			6	4	$u^6d^2(2)$
1.00 Si(1)			5	4	$u^5d^3(3)$
1.00 Si(2)			5	4	$u^5d^3(3)$

[a] The code refers to the vacancy type[5] distributed over the cubic domain in the ideal arrangement.

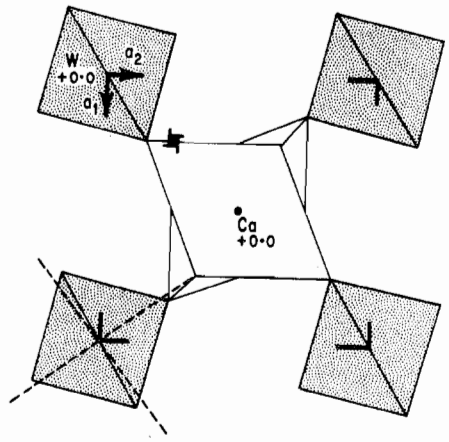

Figure 2. Unit sheet in the crystal structure of scheelite, $CaWO_4$. The WO_4 tetrahedra are stippled and the CaO_8 twisted cube is sketched unshaded. Dashed lines show the four additional W–O "bonds". Application of the 4_1-screw completes the crystal structure.

S{*pcam*} ∩ S{*p*2}, where S denotes the set of symmetry elements, we obtain S{*p*2} which is the highest admissible sheet group symmetry of the composite ideal arrangement. Performing the composition of S{*p*2} with S{$A\ 1^1/n\ 1$} yields {1,2}·{1,*A*,*a*,*n*} = {1,2,*A*,2_1,*a*,*n*,*i*(1),*i*(2)} or S{$A\ 1\ 2_1/n\ 1$}. In general, it is possible to relate a sheet group, R, to a space group, Φ, via a pole group, P, that is R·P = Φ. Here, we accept as the sheet groups the 80 "two-sided" plane groups[14] and, as pole groups, the translations along an axis or a plane normal to the plane of the sheet group. The advantage of this kind of analysis is obvious: structural relationships can be directly ascertained through decomposition of regions of a structure into plane groups, sheet groups, and pole groups and tell us just which regions of the structure require detailed description. Fluorite derivative structures, owing to the checkerboard patterns, are "lamellate"; that is they can be conceived as stacks or layers each of which is referable to a sheet group. The entire three-dimensional structure is then generated through appropriate application of a pole group.

The ideal checkerboards taken together result in space group $A2/a$ (=$A\ 1\ 2_1/n\ 1$) and the space group genealogy starting with fluorite is $F4/m\bar{3}\ 2/m \rightarrow F2/n\ 2_1/n\ 2/b \rightarrow A2/n\ 2_1/n\ 2/b$ ($2a_F$, $4a_F$, $2a_F$) $\rightarrow A1\ 2_1/n\ 1$. This involves one "zellengleich" transformation followed by a "klassengkich" transformation followed by one "zellengleich" transformation.[15] We call these *topological* transformations[16] since each discrete step involves the creation of a set of ordered vacancies over the anion frame and a new set of coordination numbers. In effect, these steps would correspond to reconstructive phase changes.

The transformation from $A\ 1\ 2_1/n\ 1 \rightarrow A\ 1\ 1/n\ 1$ is of a different kind. We can enrich our comprehension of it by appealing to the scheelite structure type $CaWO_4$, $a = 5.2$ Å, $c = 11.3$ Å, $Z = 4$, $I4_1/a$, a polyhedral diagram of which appears in Figure 2. This diagram corresponds to the asymmetric unit with one checkerboard since the 4_1-screw generates the remaining three checkerboards, completing the *c*-repeat, that is S{$p2/b$}·S{4_1} = S{$4_1/a$}. Scheelite is ideally a fluorite structure but a geometrical transformation leads to 4 + 4 coordination about W (i.e., 4 nearest neighbors and 4 next-nearest neighbors). The transformation is seen as a local movement of a tetrahedral array of oxygens toward the W atom. In effect, scheelite is a locally collapsed version of the fluorite structure type. Continuous movement of oxygens restores full eight-coordination for all cations. In scheelite, the step is one large jump: $F4/m\bar{3}\ 2/m \rightarrow I4_1/a$ ($a = a_F$, $c = 2a_F$).

Four kinds of geometrical transformations are discerned in parwelite and all involve local collapse of the oxygens. We can realize these via the Figure 3 series, which feature the polyhedral diagrams of the actual structure at $y = 0$, ${}^1/_4$, and ${}^1/_8$ levels. According to Table IV, As(1) and As(2) are diminished in their coordination from 6 (ideal) to 4 (real), M(9) and M(10) from 6 to 5, M(5) and M(6) from 7 to 6, and Si(1) and Si(2) from 5 to 4. As(1) and As(2) achieve this by displacement away from two anions each: As(1) from O(18) and O(22) and As(2) from O(13) and O(21) [Figure 3b]. For

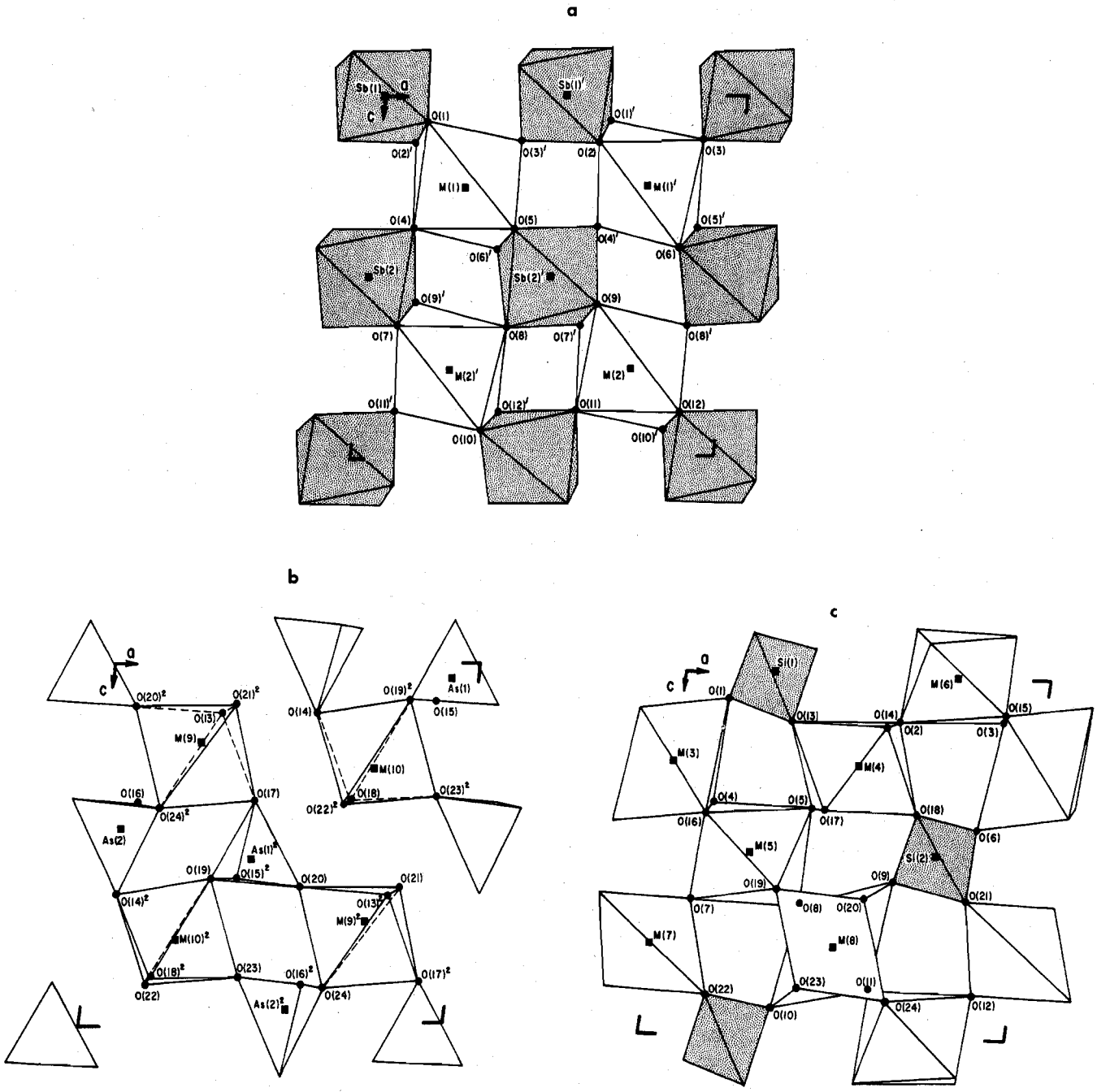

Figure 3. Three nonequivalent sheets in the real parwelite crystal structure featured as polyhedral diagrams: (a) the sheet at $y = 0$, with the SbO_6 octahedra stippled; (b) the broken sheet at $y = {}^1/_4$; (c) the sheet at $y = {}^1/_8$, with the SiO_4 tetrahedra stippled.

M(9) and M(10), O(16) and O(15), respectively, are displaced away from these cations thus reducing their coordination numbers each by 1. In Figure 3c, it is seen that O(17) is displaced away from M(5), and O(14), from M(6). Finally, O(23) is displaced away from Si(1), and O(20), from Si(2). Of particular interest is the local resemblance of the Si(1)-O_4-M(8)O_8-Si(2)O_4 arrangement to the local WO_4-Ca-O_8-WO_4 arrangement in scheelite. The geometrical coincidence, including local distortions, is noteworthy. Astute crystal chemists will also recognize the close geometrical similarity of the M(5)O_6-M(8)O_8-M(6)O_6 arrangement to the Mn(4)O_6-Mn(1)O_8-Mn(4)O_6 arrangement in braunite.[5]

Coordination Polyhedra: Bond Distances and Angles. Figure 3a reveals that at the $y \approx 0$ level, the Sb^{5+} cations are well ordered, defining a subcell, the repeat of which corresponds to the fluorite edge. The SbO_6 octahedra share edges with the MO_6 octahedra to form chains which run along the [101] direction. These chains are corner-linked to equivalent chains along [$\bar{1}$01] to form $^2_\infty[M_2Sb_2O_6]$ sheets which are local approximations to cubic close-packing and correspond to a slice of the NaCl arrangement down [110]. At $y = {}^1/_8$ (Figure 3c), complex sheets consisting of MO_8 cubes, MO_6 octahedra, and MO_4 and SiO_4 tetrahedra link by corner- and edge-sharing and further link to the $^2_\infty[M_2Sb_2O_6]$ sheets by corner- and edge-sharing. These sheets have composition $^2_\infty[M_3SiO_6]$. At $y = {}^1/_4$ (Figure 3b), sheets no longer occur, but instead $^1_\infty[M_2As_2O_6]$ double chains appear, which run parallel to [101]. The polyhedra at this level share only corners with each other. The appearance of the chains, instead of sheets, is a consequence of the geometrical displacement of As away from the oxygen atoms.

We do not consider it relevant to discuss the coordination polyhedra in great detail since their geometries obtain, to a considerable extent, from the relationship of parwelite to

Table V. Parwelite Polyhedral Interatomic Distances (Å) and Angles (deg)[a]

Sb(1)		
Sb(1)-O(11)(1)[c]	1.92 (2)	
-O(3)	1.94 (1)	
-O(2)(1)	1.96 (2)	
-O(12)	1.98 (1)	
-O(10)(1)	1.99 (2)	
-O(1)	2.13 (1)	
Average	1.99	
O(2)(1)-O(11)(1)	2.57 (3)**[b]	82.7 (9)
O(3)-O(12)	2.60 (2)**	83.1 (5)
O(1)-O(2)(1)	2.70 (3)**	82.5 (7)
O(1)-O(3)	2.70 (2)**	82.9 (5)
O(10)(1)-O(11)(1)	2.78 (3)**	90.4 (8)
O(10)(1)-O(12)	2.80 (2)**	89.7 (6)
O(3)-O(10)(1)	2.84 (2)	92.5 (6)
O(2)(1)-O(10)(1)	2.90 (2)	94.4 (8)
O(2)(1)-O(3)	2.92 (3)	96.8 (7)
O(11)(1)-O(12)	2.93 (3)	97.2 (8)
O(1)-O(11)(1)	2.97 (3)	94.2 (7)
O(1)-O(12)	2.99 (2)	93.4 (5)
Average	2.81	90.0
Sb(2)		
Sb(2)-O(5)(1)	1.95 (1)	
-O(4)	1.96 (2)	
-O(7)	1.96 (2)	
-O(8)(1)	1.97 (1)	
-O(6)	1.98 (2)	
-O(9)(1)	2.09 (1)	
Average	1.99	
O(7)-O(9)(1)	2.62 (3)**	80.6 (7)
O(4)-O(7)	2.66 (3)**	85.5 (8)
O(5)(1)-O(8)(1)	2.67 (2)**	85.6 (5)
O(4)-O(6)	2.73 (2)**	88.0 (7)
O(5)(1)-O(6)	2.76 (2)**	89.4 (6)
O(8)(1)-O(9)(1)	2.79 (2)**	87.1 (5)
O(6)-O(7)	2.87 (2)	93.4 (7)
O(4)-O(9)(1)	2.88 (2)	90.8 (7)
O(4)-O(5)(1)	2.88 (2)	94.7 (7)
O(7)-O(8)(1)	2.88 (2)	94.1 (7)
O(6)-O(8)(1)	2.89 (2)	94.1 (6)
O(5)(1)-O(9)(1)	3.02 (2)	96.6 (5)
Average	2.80	90.0
Si(1)		
Si(1)-O(13)	1.58 (2)	
-O(22)	1.60 (2)	
-O(10)	1.63 (2)	
-O(1)	1.71 (1)	
Average	1.63	
O(1)-O(13)	2.55 (2)	101.4 (9)
O(10)-O(22)	2.64 (2)	109.8 (8)
O(10)-O(13)	2.65 (2)	111.1 (9)
O(1)-O(10)	2.67 (2)	106.1 (8)
O(1)-O(22)	2.68 (2)	108.3 (8)
O(13)-O(22)	2.75 (2)	119.1 (10)
Average	2.66	109.3
Si(2)		
Si(2)-O(18)	1.61 (2)	
-O(21)	1.62 (2)	
-O(6)	1.64 (2)	
-O(9)	1.69 (2)	
Average	1.64	
O(9)-O(21)	2.58 (2)	102.8 (8)
O(6)-O(18)	2.60 (2)	106.6 (9)
O(6)-O(21)	2.65 (2)	109.0 (9)
O(6)-O(9)	2.69 (2)	108.0 (8)
O(18)-O(21)	2.74 (2)	116.6 (10)
O(9)-O(18)	2.76 (2)	113.6 (8)
Average	2.67	109.4
As(1)		
As(1)-O(19)(2)	1.62 (2)	
-O(15)	1.69 (2)	
-O(17)(2)	1.69 (2)	
-O(20)(2)	1.68	
Average	1.68	
O(19)(2)-O(20)(2)	2.56 (2)*	100.8 (8)
O(15)-O(19)(2)	2.65 (2)	106.3 (8)
O(17)(2)-O(19)(2)	2.73 (2)	111.3 (8)
O(15)-O(20)(2)	2.78 (2)	109.7 (7)
O(17)(2)-O(20)(2)	2.83 (2)	113.0 (7)
O(15)-O(17)(2)	2.84 (2)	114.7 (8)
Average	2.73	109.3
As(2)		
As(2)-O(23)(2)	1.60 (2)	
-O(14)(2)	1.66 (2)	
-O(16)	1.69 (2)	
-O(24)(2)	1.77 (1)	
Average	1.68	
O(23)(2)-O(24)(2)	2.66 (2)*	103.9 (8)
O(16)-O(24)(2)	2.68 (2)	101.1 (8)
O(16)-O(23)(2)	2.69 (3)	109.3 (9)
O(14)(2)-O(23)(2)	2.72 (3)	113.1 (9)
O(14)(2)-O(24)(2)	2.84 (3)	111.9 (9)
O(14)(2)-O(16)	2.85 (3)	116.3 (9)
Average	2.74	109.3
M(1)		
M(1)-O(4)	1.95 (2)	
-O(3)(1)	2.06 (2)	
-O(1)	2.23 (1)	
-O(5)	2.27 (1)	
-O(2)(1)	2.28 (2)	
-O(6)(1)	2.47 (2)	
Average	2.21	
O(1)-O(2)(1)	2.70 (3)**	73.6 (7)
O(5)-O(6)(1)	2.76 (2)**	71.1 (5)
O(1)-O(4)	2.88 (2)***	86.6 (7)
O(2)(1)-O(4)	2.98 (3)	89.3 (8)
O(2)(1)-O(3)(1)	2.99 (2)***	87.1 (7)
O(4)-O(5)	3.02 (2)***	90.8 (7)
O(3)(1)-O(6)(1)	3.07 (2)***	84.8 (5)
O(3)(1)-O(5)	3.14 (2)	92.6 (6)
O(4)-O(6)(1)	3.20 (2)	92.0 (7)
O(1)-O(3)(1)	3.21 (2)	96.6 (6)
O(1)-O(5)	3.69 (4)	108.1 (6)
O(2)(1)-O(6)(1)	3.77 (4)	107.2 (7)
Average	3.12	90.0
M(2)		
M(2)-O(8)(1)	2.01 (1)	
-O(7)(1)	2.12 (2)	
-O(11)	2.12 (2)	
-O(12)	2.24 (1)	
-O(9)	2.38 (1)	
-O(10)(1)	2.42 (2)	
Average	2.21	
O(7)(1)-O(9)	2.62 (3)**	70.9 (7)
O(10)(1)-O(12)	2.80 (2)**	73.8 (5)
O(7)(1)-O(8)(1)	2.92 (2)***	89.8 (7)
O(9)-O(11)	2.98 (3)***	82.6 (7)
O(11)-O(12)	2.99 (2)***	86.5 (7)
O(7)(1)-O(11)	3.05 (3)	91.8 (9)
O(8)(1)-O(10)(1)	3.05 (2)***	86.1 (6)
O(8)(1)-O(12)	3.06 (2)	91.7 (6)
O(8)(1)-O(9)	3.28 (2)	96.4 (6)
O(10)(1)-O(11)	3.35 (3)	94.8 (7)
O(9)-O(12)	3.70 (4)	104.1 (5)
O(7)(1)-O(10)(1)	3.70 (4)	111.2 (7)
Average	3.12	90.0
M(3)		
M(3)-O(15)	2.07 (2)	
-O(3)	2.08 (1)	
-O(16)	2.13 (2)	
-O(4)	2.14 (2)	
-O(1)	2.37 (1)	
-O(6)	2.57 (2)	
Average	2.23	
O(3)-O(15)	2.69 (2)***	80.8 (6)
O(1)-O(3)	2.70 (2)**	74.3 (5)
O(4)-O(6)	2.73 (2)**	70.2 (6)
O(1)-O(4)	2.88 (2)***	79.1 (6)
O(4)-O(16)	2.89 (3)***	85.0 (7)
O(3)-O(4)	3.04 (1)	92.1 (3)
O(3)-O(6)	3.07 (2)***	81.9 (5)
O(1)-O(15)	3.26 (2)	94.4 (5)
O(15)-O(16)	3.28 (1)	102.6 (3)
O(6)-O(16)	3.36 (2)	90.7 (6)
O(1)-O(16)	3.76 (3)	111.7 (6)
O(6)-O(15)	3.84 (4)	113.0 (6)
Average	3.13	89.7
M(4)		
M(4)-O(5)	2.13 (2)	
-O(13)	2.15 (2)	
-O(18)	2.16 (2)	
-O(2)	2.18 (2)	
-O(17)	2.41 (2)	
-O(14)	2.43 (2)	
Average	2.24	
O(13)-O(17)	2.89 (2)***	78.4 (6)
O(14)-O(18)	2.93 (3)***	79.3 (7)
O(14)-O(17)	2.93 (1)	74.4 (3)
O(2)-O(18)	3.01 (3)	88.1 (7)
O(13)-O(14)	3.03 (3)	82.6 (7)
O(5)-O(13)	3.05 (2)	91.3 (6)
O(17)-O(18)	3.10 (2)	85.2 (6)
O(2)-O(5)	3.20 (1)	96.2 (4)
O(5)-O(17)	3.33 (2)	94.5 (6)
O(5)-O(18)	3.37 (2)	104.1 (6)
O(2)-O(14)	3.40 (3)	95.1 (8)
O(2)-O(13)	3.44 (3)	105.5 (8)
Average	3.14	89.6
M(5)		
M(5)-O(19)	2.16 (2)	
-O(16)	2.20 (2)	
-O(7)	2.22 (2)	
-O(5)	2.23 (1)	
-O(4)	2.23 (2)	
-O(8)	2.24 (1)	
Average	2.21	
O(4)-O(7)	2.66 (3)**	73.4 (7)
O(5)-O(8)	2.67 (2)**	73.2 (5)
O(16)-O(19)	2.88 (2)	82.6 (7)
O(4)-O(16)	2.89 (3)***	81.3 (7)
O(7)-O(8)	2.92 (3)***	81.7 (6)
O(8)-O(19)	3.01 (2)***	86.3 (6)
O(4)-O(5)	3.02 (2)***	84.9 (6)
O(7)-O(16)	3.37 (3)	99.1 (7)
O(5)-O(19)	3.46 (2)	103.9 (6)
O(7)-O(19)	3.51 (3)	106.3 (7)
O(4)-O(8)	3.65 (3)	109.5 (6)
O(5)-O(16)	3.67 (4)	111.7 (6)
Average	3.14	91.2

Table V (*Continued*)

M(6)		
M(6)-O(24)	2.07 (2)	
-O(3)	2.15 (1)	
-O(11)	2.17 (2)	
-O(15)	2.19 (2)	
-O(12)	2.22 (1)	
-O(2)	2.23 (2)	
Average	2.17	
O(2)-O(11)	2.57 (3)**	71.4 (8)
O(3)-O(12)	2.60 (2)**	73.0 (5)
O(3)-O(15)	2.69 (2)***	76.6 (6)
O(11)-O(24)	2.85 (3)***	84.6 (8)
O(15)-O(24)	2.93 (2)	87.0 (6)
O(2)-O(3)	2.99 (2)***	86.4 (6)
O(11)-O(12)	2.99 (2)***	85.7 (7)
O(12)-O(15)	3.18 (2)	92.4 (5)
O(12)-O(24)	3.35 (2)	102.4 (6)
O(2)-O(24)	3.43 (3)	105.9 (7)
O(3)-O(11)	3.56 (2)	111.2 (7)
O(2)-O(15)	3.72 (4)	114.8 (7)
Average	3.07	91.0

M(7)		
M(7)-O(22)	2.04 (1)	
-O(12)	2.04 (1)	
-O(21)	2.07 (2)	
-O(7)	2.15 (2)	
Average	2.07	
O(12)-O(22)	3.14 (2)	100.6 (6)
O(12)-O(21)	3.14 (2)	99.8 (6)
O(7)-O(22)	3.17 (2)	98.3 (6)
O(7)-O(12)	3.18 (1)	98.5 (4)
O(7)-O(21)	3.38 (3)	106.3 (8)
O(21)-O(22)	3.92 (4)	145.0 (4)
Average	3.32	108.1

M(8)		
M(8)-O(8)	2.19 (1)	
-O(11)	2.22 (2)	
-O(20)	2.26 (1)	
-O(24)	2.42 (1)	
-O(23)	2.50 (2)	
-O(19)	2.52 (2)	
-O(9)	2.54 (1)	
-O(10)	2.72 (2)	
Average	2.42	
O(19)-O(20)	2.56 (2)*	64.6 (6)
O(23)-O(24)	2.66 (2)*	65.3 (5)
O(20)-O(24)	2.73 (2)***	71.4 (5)
O(10)-O(11)	2.78 (3)**	67.7 (7)
O(8)-O(9)	2.79 (2)**	72.1 (5)
O(11)-O(24)	2.85 (3)***	75.7 (7)
O(19)-O(23)	2.85 (2)***	69.1 (6)
O(9)-O(20)	2.91 (2)	74.6 (5)
O(9)-O(11)	2.98 (3)***	77.1 (7)
O(8)-O(19)	3.01 (2)***	78.9 (5)
O(10)-O(23)	3.03 (2)	70.8 (6)
O(8)-O(10)	3.05 (2)***	75.9 (5)
Average	2.85	71.9

M(9)		
M(9)-O(21)(2)	2.02 (2)	
-O(13)	2.04 (2)	
-O(17)	2.08 (2)	
-O(20)(2)	2.08 (2)	
-O(24)(2)	2.25 (1)	
Average	2.09	
p O(20)(2)-O(24)(2)	2.73 (2)	78.3 (6)
p O(20)(2)-O(21)(2)	2.75 (2)	84.4 (7)
p O(17)-O(24)(2)	2.87 (2)	82.8 (6)
p O(13)-O(17)	2.89 (2)***	89.2 (7)
p O(17)-O(21)(2)	3.11 (2)	98.7 (7)
m O(21)(2)-O(24)(2)	3.24 (2)	98.3 (7)
p O(13)-O(20)(2)	3.31 (2)	107.4 (7)
m O(13)-O(21)(2)	3.33 (3)	110.2 (8)
m O(13)-O(24)(2)	4.18 (4)	151.3 (6)
a O(17)(2)-O(20)	*d*	161.1 (7)

M(10)		
M(10)-O(23)(2)	2.03 (2)	
-O(18)	2.05 (2)	
-O(22)(2)	2.09 (1)	
-O(14)	2.15 (2)	
-O(19)(2)	2.28 (2)	
Average	2.12	
p O(19)(2)-O(23)(2)	2.85 (2)***	82.4 (7)
p O(14)-O(19)(2)	2.86 (3)	80.1 (7)
p O(22)(2)-O(23)(2)	2.90 (2)	89.3 (6)
p O(14)-O(18)	2.93 (3)	88.6 (7)
p O(14)-O(22)(2)	3.15 (3)	95.8 (7)
p O(18)-O(23)(2)	3.23 (2)	104.8 (7)
m O(19)(2)-O(22)(2)	3.39 (2)	101.4 (6)
m O(18)-O(22)(2)	3.46 (3)	113.6 (7)
m O(18)-O(19)(2)	4.10 (3)	144.1 (7)
a O(14)-O(23)(2)	*d*	162.4 (7)

[a] Estimated standard deviation refers to the last digit. [b] Oxygen polyhedral shared edges: one asterisk, As-M; two asterisks, Sb-M; three asterisks, M-M. [c] (1) = $^1/_2 + x, -y, z$, applied to coordinates in Table III; (2) = $^1/_2 + x, ^1/_2 - y, ^1/_2 + z$, applied to coordinates in Table III. [d] Not available.

fluorite. For example, arrangements of the type $u^6d^2(2)$ and $u^6d^2(3)$, although they formally represent octahedral coordination, exhibit different types of distortion owing to the nonisomorphism of the two with respect to ordered vacancies on the cube. Polyhedral distortions also result from the presence of shared edges between them and, as seen in Table V, these are usually the shortest edges. Finally, the geometrical displacements away from the ideal fluorite framework must be taken into account for, as Table III shows, these range from 0.06 Å (M(1)) to 1.17 Å (O(14)). The average displacement for the cations at $y \approx 0$ is 0.08 Å; at $y \approx {}^1/_8$, 0.24 Å; and at $y \approx {}^1/_4$, 0.60 Å. For O(1) through O(12) at $y \approx {}^1/_{16}$, the average displacement is 0.47 Å; and for O(13) through O(24) at $y \approx {}^3/_{16}$, this is 0.70 Å. The definition of true coordination number is somewhat blurred in a crystal structure such as parwelite since vacancies occur over the anion frame and not over the cations (in the crystallographic dense-packings, the vacancies occur over the cation frame with the dense-packed anions fully occupied). Mn^{2+}, for example, possesses known coordination numbers from 4 to 8 in oxide environments, and the range of individual distances, particularly for coordination numbers greater than 6, can be substantial. To properly assign coordination numbers, we took the ideal arrangement, the polyhedral averages, and the bond length–bond strength correlations into account. Table VI lists for all 24 nonequivalent oxygens, the deviation Δp_0 of bond strength sums of cation coordination polyhedra from local electrostatic neutrality and the corresponding deviation, Δd, in individual bond distances from polyhedral averages.[17]

Writing coordination numbers in brackets, the average polyhedral distances are $^{[6]}Sb(1)-O = 1.99$, $^{[6]}Sb(2)-O = 1.99$, $^{[6]}M(1)-O = 2.21$, $^{[6]}M(2)-O = 2.21$, $^{[6]}M(3)-O = 2.23$, $^{[6]}M(4)-O = 2.24$, $^{[6]}M(5)-O = 2.21$, $^{[6]}M(6)-O = 2.17$, $^{[4]}M(7)-O = 2.07$, $^{[8]}M(8)-O = 2.42$, $^{[5]}M(9)-O = 2.09$, $^{[5]}M(10)-O = 2.12$, $^{[4]}Si(1)-O = 1.63$, $^{[4]}Si(2)-O = 1.64$, $^{[4]}As(1)-O = 1.68$, and $^{[4]}As(2)-O = 1.68$ Å. Except for M(8)–O and M(9)–O, these distances are typical averages for coordination polyhedra of similar cations in other crystals.[18] The $^{[8]}M(8)-O$ average is about 0.09 Å longer than that found for $^{[8]}Mn^{2+}-O$ in braunite[5] and we suspect this may result from preferential substitution of Ca^{2+} reported in the chemical analysis and from the long M(8)–O(10) = 2.72 Å distance, the latter obtaining from substantial cation oversaturation ($\Delta p_{O(10)} = +0.42$). The $M(8)O_8$ polyhedron is a twisted cube, similar to the polyhedra found in braunite, pyrochlore, scheelite, and garnets. The $^{[5]}M(9)-O$ distance is shorter than $^{[5]}Mn^{2+}-O = 2.12$ Å found[19] in eveite, $^{[6]}Mn^{II}(^{[5]}Mn^{II})(OH)(AsO_4)$; site population refinement, discussed earlier, suggests that substantial Mg^{2+} (49%) substitutes at this site. The $M(7)O_4$ polyhedron must be accepted as a highly distorted tetrahedron since a fifth M(7)–O distance is greater than 3.6 Å. Its distortion is rather severe with O(21)–M(7)–O(22) = 145.0°. This arises from the fact that parwelite is a fluorite derivative structure where the oxygen environment is constrained by the environment of other cations as well. $M(9)O_5$ and $M(10)O_5$ are interpreted as highly distorted trigonal

Table VI. Correlations in Bond Strength Sum Deviations (Δp_0) with Bond Length Deviations (Δd) for Parwelite[a]

Anion		Sb(1)	Sb(2)	M(1)	M(2)	M(3)	M(4)	M(5)	M(6)	M(7)	M(8)	M(9)	M(10)	Si(1)	Si(2)	As(1)	As(2)
O(1)	+0.50	+0.14		+0.02		+0.14								+0.08			
O(2)	−0.17	−0.03		+0.07			−0.06		+0.06								
O(3)	−0.17	−0.09		−0.15		−0.15			−0.12								
O(4)	−0.17		−0.03	−0.26		−0.09		+0.02									
O(5)	−0.17		−0.04	+0.06			−0.11	+0.02									
O(6)	+0.50		−0.01	+0.26		+0.34									+0.00		
O(7)	+0.00		−0.03		−0.09			+0.01		+0.08							
O(8)	−0.25		−0.02		−0.20			+0.03			−0.23						
O(9)	+0.42		+0.10		+0.17						+0.12				+0.05		
O(10)	+0.42	+0.00			+0.21						+0.30			+0.00			
O(11)	−0.25	−0.07			−0.09				+0.00		−0.20						
O(12)	+0.00	−0.01			+0.03				+0.05	−0.03							
O(13)	−0.27						−0.09					−0.05		−0.05			
O(14)	−0.02						+0.19						+0.03				−0.02
O(15)	−0.08					−0.16			+0.02							+0.01	
O(16)	−0.08					−0.10		−0.01									+0.01
O(17)	−0.02						+0.17					−0.01				+0.01	
O(18)	−0.27						−0.08						−0.07		−0.03		
O(19)	+0.23							−0.05			+0.10		+0.16			−0.06	
O(20)	−0.10										−0.16	−0.01				+0.03	
O(21)	−0.10									+0.00		−0.07			−0.02		
O(22)	−0.10									−0.03			−0.03	−0.03			
O(23)	−0.10										+0.08		−0.09				−0.08
O(24)	+0.23								−0.10		+0.00	+0.16					+0.09

[a] The bond length deviations from polyhedral averages, Δd, are listed under the appropriate cation and anion.

bipyramids. Three kinds of bonds are distinguished: six correspond to the edges of the bipyramid (p), three to the trigonal meridion (m), and one to the trigonal bipyramidal axis (a). For an ideal trigonal bipyramid, these should be p = 90°, m = 120°, and a = 180° where the angles are taken as O–M–O′ identified with these edges.[20] Five-coordination presents a problem since there are two limiting convex polyhedra, the trigonal bipyramid and the square pyramid, and neither is a regular solid. Distortions can be considered as a "solid–solution" between the two limiting cases.

The bond strength–bond length correlations in Table VI are in generally good agreement. For example O(1), O(6), O(9), and O(10), which are all considerably oversaturated ($\Delta p_0 >$ 0.42), reveal individual distances to bonded cations which are longer than average. The anions whose bond strength sum deviations are small possess deviations in distances which compensate and balance each other. These calculations add credence to the coordination number assignments and, furthermore, confirm the statement that parwelite is in fact an anhydrous complex oxide.

Discussion

These observations on parwelite, which is perhaps the most complicated fluorite derivative structure to date, add much to our understanding of the subtle interrelationships among structure types. In parwelite, we see "islands" of structure closely related to regions of other seemingly unrelated structures but more important we recognize that two kinds of transformations obtain in passing from a parent structure to its derivatives. The geometrical transformations correspond to displacive phase changes and suggest that compounds like parwelite and scheelite may exhibit continuous changes in coordination number as a function of temperature and pressure. The topological transformations correspond to reconstructive phase changes for topological bonds are broken through removal of anions in the framework. Both transformations lead to structures which are "infinitely adaptive"[21] and, through systematic removal of anions from the fluorite frame, a wide range of coordination numbers obtains, admitting a great variety of cations into their structures. This great versatility is one of the reasons mineral structures tend to be complicated, since the pool of cations draws from systems with a large number of components. Parwelite is remarkable in exhibiting Mn^{2+} in coordination numbers 4, 5, 6, and 8. Evidence is accumulating that the list of fluorite derivative structures is impressively long but, owing to grotesque stoichiometry, complex supercells often of low symmetry, and gross physical similarity among the species, such compounds have been poorly characterized at best.

Let us remark finally that further study on complex oxides and oxyfluorides derived from fluorite has much promise but requires extreme caution. Analysis of the weak superstructure reflections will prove to be the key to understanding these structures. The distinction between topological transformations and geometrical transformations, we believe, is important. Perhaps most frustrating to the investigator is the physical similarity among these compounds: they are highly refractory, are brittle and without prominent cleavages, and are relatively dense, much resembling the garnets in appearance. Owing to the dominance of the fluorite substructure in the observed intensity distributions, even their powder patterns are similar to each other. Of all known inorganic compounds, these complex oxides are perhaps the most resistant to formal structural description and classification and for this reason there exists no adequate treatment in the standard pedagogical treatises. We wonder how many such compounds, both natural and synthetic, still remain hidden from us owing to their strong mimetic character.

Acknowledgment. We appreciate the collection of the data set by Dr. G. D. Brunton, who was assisted by Dr. P. K. SenGupta. Our portion of the study was supported by National Science Foundation Grant GA-40543 and a Materials Research Laboratory grant (NSF) awarded to The University of Chicago.

Registry No. Parwelite, 12420-60-9.

Supplementary Material Available: Listing of structure factor amplitudes (11 pages). Ordering information is given on any current masthead page.

References and Notes

(1) P. B. Moore, *Ark. Mineral. Geol.*, **4**, 467 (1968).
(2) P. B. Moore, *Mineral. Rec.*, **1**, 154 (1970).
(3) S. Geller, *Acta Crystallogr., Sect. B*, **27**, 821 (1971).
(4) J. P. R. de Villiers, *Am. Mineral.*, **60**, 1098 (1975).
(5) P. B. Moore and T. Araki, *Am. Mineral.*, **61**, 1226 (1976).
(6) P. B. Moore and T. Araki, *Inorg. Chem.*, **15**, 316 (1976).
(7) T. Srikrishnan and S. Parthasarathy, *Z. Kristallogr., Kristallgeom., Kristallphys., Kristallchem.*, **131**, 186 (1970).
(8) G. N. Ramachandran and R. Srinivasan, "Fourier Methods in Crystallography", Wiley-Interscience, New York, N.Y., 1970, p 96.
(9) D. T. Cromer and J. B. Mann, *Acta Crystallogr., Sect. A*, **24**, 321 (1968).

(10) D. T. Cromer and D. Liberman, Report LA-4403, UC-34, Los Alamos Scientific Laboratory, University of California, Berkeley, Calif., 1970.
(11) W. H. Zachariasen, *Acta Crystallogr., Sect. A*, **24**, 212 (1968).
(12) L. W. Finger, *Carnegie Inst. Washington, Yearb.*, **67**, 216 (1969).
(13) G. Pólya, *Acta Math.*, **68**, 146 (1937).
(14) W. T. Holser, *Z. Kristallogr., Kristallgeom., Kristallphys., Kristallchem.*, **110**, 266 (1958).
(15) J. Neubüser and H. Wondratschek, *Krist. Tech.*, **1**, 530 (1966).
(16) P. B. Moore and T. Araki, *Am. Mineral.*, **61**, 74 (1976).
(17) W. H. Baur, *Trans. Am. Crystallogr. Assoc.*, **6**, 129 (1970).
(18) R. D. Shannon and C. T. Prewitt, *Acta Crystallogr., Sect. B*, **25**, 925 (1969).
(19) P. B. Moore and J. R. Smyth, *Am. Mineral.*, **53**, 1841 (1968).
(20) D. A. Stephenson and P. B. Moore, *Acta Crystallogr., Sect. B*, **24**, 1518 (1968).
(21) J. S. Anderson, *J. Chem. Soc., Dalton Trans.*, 1107 (1973).

Contribution from the Department of Chemistry, University of Virginia, Charlottesville, Virginia 22901

Crystal and Molecular Structure of a Tetracarbon Carborane, $(CH_3)_4C_4B_8H_8$, a New Type of Nido Cage System

DEREK P. FREYBERG, RICHARD WEISS, EKK SINN, and RUSSELL N. GRIMES*

Received January 18, 1977 AIC70032K

The structure of 2,3,7,8-tetramethyl-2,3,7,8-tetracarbadodecaborane(12) $[(CH_3)_4C_4B_8H_8]$, a carborane formed by air oxidation of $[(CH_3)_2C_2B_4H_4]_2CoH$ or $[(CH_3)_2C_2B_4H_4]_2FeH_2$, has been determined from a single-crystal x-ray diffraction study. The molecule is a distorted icosahedron, in which two carbon–carbon bonds have been severed to create two four-sided open faces, and consists of two pyramidal $(CH_3)_2C_2B_4H_4$ units fused face-to-face with the four skeletal carbon atoms forming a contiguous chain. The polyhedral cage contains two more electrons than the icosahedral $C_2B_{10}H_{12}$ system and is isoelectronic with the $C_2B_{10}H_{12}^{2-}$ ion. The geometry of $(CH_3)_4C_4B_8H_8$ differs sharply from those of the only other structurally established 12-vertex nido systems, $(C_6H_5)_2C_2B_{10}H_{11}^-$ and $(\eta^5\text{-}C_5H_5)Fe(CH_3)_4C_4B_7H_8$, each of which has a single large open face. The compound crystallizes in the monoclinic space group $P2_1/n$ with $a = 8.398$ (3) Å, $b = 11.420$ (5) Å, $c = 13.458$ (7) Å, $\beta = 90.61$ (4)°, $d_{obsd} = 1.05$ g cm^{-3}, and $d_{calcd} = 1.04$ g cm^{-3} for $Z = 4$. The structure was refined by full-matrix least-squares procedures to a final R value of 0.153. The molecule is discussed in relation to the theory of bonding in polyhedral cages and also in terms of the mechanism of its formation from the metallocarborane precursors.

In earlier papers from this laboratory[1,2] we described the preparation and spectroscopic characterization of a new carborane $(CH_3)_4C_4B_8H_8$ and its use as a ligand in tetracarbon metallocarboranes. Although nearly 3 years has elapsed since its discovery, definitive structural characterization of this molecule eluded us despite the fact that it is an air-stable solid which can be obtained in high yield and purity from the readily prepared complexes[2,3] $[(CH_3)_2C_2B_4H_4]_2FeH_2$ and $[(CH_3)_2C_2B_4H_4]_2CoH$. The proton and boron-11 NMR spectra of $(CH_3)_4C_4B_8H_8$ are complicated by its strange behavior in solution,[1,2] in which an equilibrium is established between two structurally distinct isomers, A and B, one of which (B) is fluxional above 25 °C; on removal of solvent, the compound reverts to a single isomer, A.

The colorless, slightly volatile crystals of A which were grown from various solvents were consistently unsuitable for x-ray structural analysis. Nevertheless, an x-ray study of this compound remained an objective of high priority for several reasons: (1) The molecule contains two more skeletal electrons than the icosahedral $C_2B_{10}H_{12}$ system, and a structural comparison with the latter molecule was a matter of considerable interest. (2) No carborane having more than two carbon atoms in the same polyhedron had been crystallographically characterized (the small species $C_4B_2H_6$ and $(CH_3)_6C_4B_2$ have been examined respectively by microwave[4] and electron diffraction[5] spectroscopy). (3) The formation of $(CH_3)_4C_4B_8H_8$ by oxidative fusion of $(CH_3)_2C_2B_4H_4^{2-}$ ligands from the above-mentioned cobalt and iron complexes[2,3] is a novel and potentially significant synthetic process whose steric details warrant examination. (4) Recent synthetic work has shown that $(CH_3)_4C_4B_8H_8$ is the prototype of a large family of tetracarbon carborane[6] and metallocarborane[7,8] cage systems.

After many attempts entailing considerable difficulty we succeeded in obtaining a few usable crystals, which were still of relatively poor quality but which did permit x-ray determination of the cage geometry and connectivity. Data collection, solution, and refinement were conducted on two crystals grown from separate samples of the compound, yielding the results which we now report.

Experimental Section

Repeated attempts to grow single crystals from a variety of common solvents produced only soft needles which were very poor diffractors of x rays and could not be used for data collection. Eventually, very slow evaporation from hexane solution over a period of weeks produced relatively hard rhomboids which gave diffraction photographs of satisfactory quality. The first crystal selected was mounted on a glass fiber open to the air. The Enraf-Nonius program SEARCH was used to obtain 15 accurately centered reflections which were then employed in the program INDEX to obtain appropriate cell dimensions and an orientation matrix for data collection. Refined cell dimensions and their estimated standard deviations were obtained from least-squares refinement of 28 accurately centered reflections. The mosaicity of the crystal was examined by the ω-scan technique and judged acceptable. Crystal data for $C_8B_8H_{20}$ are as follows: mol wt 202.7; space group $P2_1/n$; $a = 8.398$ (3), $b = 11.420$ (5), $c = 13.458$ (7) Å; $\beta = 90.61$ (4)°; $V = 1291$ Å^3; $Z = 4$; $d_{calcd} = 1.04$, $d_{obsd} = 1.05$ g cm^{-3}; μ(Mo Kα) = 0.5 cm^{-1}.

The space group chosen, $P2_1/n$, is an alternative setting of the conventional space group $P2_1/c$ (No. 14) and has the general equivalent positions x, y, z; $-x, -y, -z$; $^1/_2 + x, ^1/_2 - y, ^1/_2 + z$; $^1/_2 - x, ^1/_2 + y, ^1/_2 - z$.

Collection and Refinement of the Data. Diffraction data were collected at 292 K on an Enraf-Nonius four-circle CAD-4 diffractometer controlled by a PDP-8/M computer, using Mo Kα radiation from a highly oriented graphite crystal monochromator. The θ–2θ scan technique was used to record the intensities for all nonequivalent reflections for which $1 < 2\theta < 44°$. The scan widths (SW) used are given by SW = $A + B \tan \theta$, where A is estimated from the mosaicity of the crystal and B allows for the increase in peak width due to Kα_1–Kα_2 splitting. The values of A and B were 0.70 and 0.30°, respectively. The calculated scan angle was extended at each side by 25% for background determination (BG1 and BG2). The net count was then calculated as NC = TOT − 2(BG1 + BG2) where TOT is the calculated peak intensity. Intensities which registered less than 8 counts above background on a rapid prescan were considered insignificant and were rejected automatically by the computer.